Pressure-induced Mott insulator-metal transition and structural phase transitions in the triangular antiferromagnet $NiGa_2S_4$

Runxi Huang,[1] Min Zhang,[1,*] Chao An,[1] Ying Zhou,[1] Yonghui Zhou,[2] Xuliang Chen,[2] and Zhaorong Yang[1,2,3,†]

[1]*Institutes of Physical Science and Information Technology, Anhui University, Hefei 230601, China*

[2]*Anhui Province Key Laboratory of Condensed Matter Physics at Extreme Conditions, High Magnetic Field Laboratory, Chinese Academy of Sciences, Hefei 230031, China*

[3]*Collaborative Innovation Center of Advanced Microstructures, Nanjing 210093, China*

(Received 20 February 2023; revised 28 March 2023; accepted 6 April 2023; published 19 April 2023)

Mott insulator $NiGa_2S_4$ has attracted much attention because of its elusive magnetic ground state due to the geometric frustration and layered structures. To our knowledge, however, additional studies of the turning properties through external parameters are rather scarce in this system. Here, we comprehensively performed high-pressure studies for the $NiGa_2S_4$ single crystal. With synchrotron x-ray diffraction and Raman-scattering results, we found the starting trigonal $P\bar{3}m1$ phase quickly transfers to the $R3m$ phase at a lower pressure of 1.6 GPa due to the intralayer sliding. With further compressing, another two structural phase transitions were observed, $NiGa_2S_4$ transfers to tetragonal $P\bar{4}2m$ phase at 15.5 GPa and then enters into orthogonal $Pna2_1$ phase beyond 18.2 GPa. In addition, electrical transport measurements show a Mott insulator-metal transition close to 17 GPa, which can be related to the $R3m \rightarrow P\bar{4}2m$ transition where a $\sim$17.5% collapse in the unit-cell volume and a sharp reduction in Raman intensity occur. The metallic $NiGa_2S_4$ shows no superconducting transition down to 1.8 K. This paper enriches our understanding of $NiGa_2S_4$ especially its structure information, the tuning between the Mott insulating state and metallic state simultaneously accompanied by a structural phase transition sheds light on further understanding of magnetism and Mott physics in $NiGa_2S_4$.

DOI: 10.1103/PhysRevB.107.144106

I. INTRODUCTION

Mott insulator-metal transition (IMT) also called Mott transition, driven by strong electron-electron repulsion interaction, is a key issue in condensed-matter physics, partially because it is entangled with the mystery of the high-temperature superconductor [1]. Especially, in the frustrated Mott insulators, strong quantum fluctuation prevents conventional spin order at zero temperature and results in exotic states, such as quantum spin liquid (QSL) [2–4]. The spin-disordered state may also have hidden orders, such as spin nematic order [5], vortex topological order [6], chiral orders [7], etc. In fact, the high-temperature superconducting phase in the cuprates or iron pnictides is in close proximity to these exotic magnetic states. From the view point of Anderson, a resonating valence-bond QSL will naturally become to be superconducting if the material could be driven into conducting by pressure or doping [8]. There have already been some reports of pressure-induced superconductivity in the QSL candidates, e.g., k-$(ET)_2Cu_2(CN)_3$ [9] and $NaYbSe_2$ [10,11]. In addition to the emergent superconductivity, the Mott insulator also displays fascinating phenomena under high pressure, including the experimental findings of magnetic order in $ZnCu_3(OH)_6Cl_2$ [12,13] and $Tb_2Ti_2O_7$ [14], non-Fermi-liquid conducting state in $BaVS_3$ [15] and $PrNiO_3$ [16], IMT in MnS_2 [17] and $CrGeTe_3$ [18], etc.

The Mott insulator $NiGa_2S_4$ is an example of strongly frustrated two-dimensional triangular antiferromagnet. In $NiGa_2S_4$, magnetic correlations start to develop below $T_w \sim$ 80 K, but no long-range spin order forms even down to zero temperature [19,20]. Instead, spin fluctuations show a slowing down below $\sim$50 K with short-range incommensurate order and spin-freezing occurs at $T \sim 8.5$ K, which can be accounted for by the combination of strong third-nearest-neighbor antiferromagnetic exchange J_3 and weak nearest-neighbor ferromagnetic exchange J_1 [21,22]. Most models suggest spin-nematic order in this system, which derivates from the large quadrupole coupling [23–25]. Recently, Valentine *et al.* proposed that sulfur vacancies induce a disordered Dzyaloshinskii-Moriya interaction and then play a critical role on the absence of long-range magnetic order [26]. $NiGa_2S_4$ crystallized with the symmetry of space-group $P\bar{3}m1$ (No. 164), the Ni^{2+} ions arrange in a perfect triangular lattice with the octahedral S2-Ni-S2 layer sandwiched between two layers of tetrahedral S1-Ga-S2 layers, forming a strong two-dimensional slab separated by van der Waals force [see Figs. 1(a) and 1(b)]. The central S2-Ni-S2 plane is isostoichiometric with NiS_2, a canonical Mott insulator which undergoes an IMT at a lower pressure of ca. 3.0 GPa. Thus, it may be possible to drive $NiGa_2S_4$ into the conducting state through the path of pressure, however, the experimental investigation is still lacking [27,28].

*Corresponding author: mzhang@ahu.edu.cn

†Corresponding author: zryang@issp.ac.cn

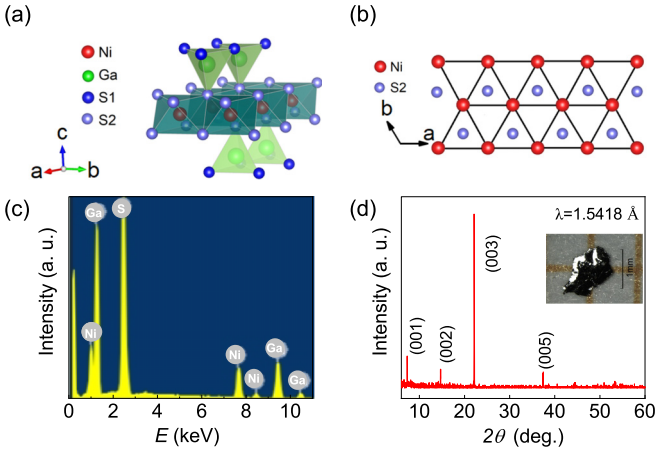

FIG. 1. Structure and characterizations of the $NiGa_2S_4$ single crystal. (a) The schematics of the crystal structure. (b) Top view of the Ni-S2 triangular lattice. (c) The EDS of the $NiGa_2S_4$ single crystal. (d) XRD pattern of the $NiGa_2S_4$ single crystal. The inset is the optical image of one typical piece of the $NiGa_2S_4$ sample.

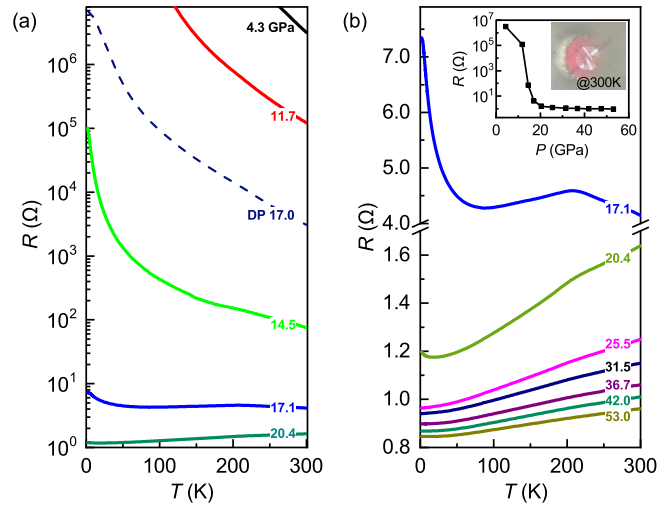

FIG. 2. Temperature dependent resistance of the $NiGa_2S_4$ single crystal at (a) lower pressure with the logarithmic scale and (b) higher pressure for the metallic phase. The inset displays the room-temperature resistance vs pressure and a photograph of the electrode configuration inside the DAC. The dashed line in (a) corresponds to the decompressing curve at 17 GPa where the returning insulator can be obviously observed.

In this paper, we experimentally explored the high-pressure behavior of the $NiGa_2S_4$ single crystal up to 53 GPa by means of electrical transport, synchrotron x-ray diffraction (XRD) and Raman-scattering measurements. We present $NiGa_2S_4$ undergoes series of structural phase transitions under high pressure, and a reversible IMT was observed accompanying with the structural change from layered trigonal phase to tetragonal phase. $NiGa_2S_4$ supports a new platform to study the correlations between IMT and the complex degrees of freedom.

II. EXPERIMENTAL METHODS

Single crystals of $NiGa_2S_4$ were prepared by chemical vapor transport method in evacuated quartz ampoules [29]. The chemicals were mixed with the molar ratio of Ni:Ga: S = 1 : 2 : 4. The transport reactions were carried out in a temperature gradient 925–850° C using a transport agent concentration of 0.1 g/cm^3 iodine. After a reaction time of 10 days, platelike crystals with areas up to 2 mm^2 and thicknesses of about 1 mm were obtained.

The stoichiometric ratio was determined by the energy dispersive spectroscopy (EDS), Fig. 1(c) shows the chemical composition value of Ni:Ga:S as ∼0.9:2:4, a slight deviation from the designed stoichiometric ratio. XRD with Cu $K\alpha$ radiation (Rigaku, TTR III) was used for crystal phase identification. In Fig. 1(d), the XRD pattern shows strong (00n) peaks, indicating the perfect crystallization of the $NiGa_2S_4$ single crystal perpendicular to the c axis.

For all high-pressure experiments, diamond anvil cell (DAC) with a pair of 300 μm-culet diamonds were utilized to generate high pressure and a predrilled rhenium gasket was used as the sample chamber. The pressure values were determined through the fluorescence shift of ruby. For the electrical transport experiments, a mixture of epoxy and cubic boron nitride powder was added to the hole, and then compressed firmly to insulate the electrodes from the gasket. Four platinum sheets were linearly arranged as the electrodes with a standard four-probe method to perform the resistance measurement as seen in Fig. 2(b). The $R-T$ curves were measured at a home-design physical property measurement system in the temperature range of 1.8–300 K. Raman spectra were collected using the Renishaw inVia Raman spectrometer system in the backscattering configuration, and the 633 nm He-Ne laser was used as the excitation light. For both electrical transport and Raman-scattering measurements, sodium chloride powders were used as the pressure transmitting medium (PTM). Synchrotron XRD were performed on the beamline 15U1 of the Shanghai Synchrotron Radiation Facility (Shanghai), and a monochromatic x-ray beam with a wavelength of 0.6199 Å was used. The powder samples were obtained from the grinding of the as-grown single crystals. Daphne 7373 oil were used as the PTM.

III. RESULTS AND DISCUSSION

A. Electrical transport

We first carried out electrical resistance measurements on $NiGa_2S_4$ single crystal up to a maximum of 53 GPa. An insulating behavior can be clearly observed in the temperature-dependent resistances at moderate pressure as seen in Fig. 2(a). As shown in Fig. 2(b), the room-temperature resistances continuously decrease with increasing pressure and reveal a drop by six orders of magnitude near 20 GPa. Above 20.4 GPa the resistance decreases with decreasing temperature, indicating an IMT occurring. For 17.1 GPa, one intermediate state can be captured by the broad peak in the resistance around 210 K, which might be a result of the mixed phases as discussed in the following XRD and Raman-scattering results. The metallic behavior persists until the maximum pressure value of 53 GPa in our experiments. With decompression, the reversibility of the transition is proposed

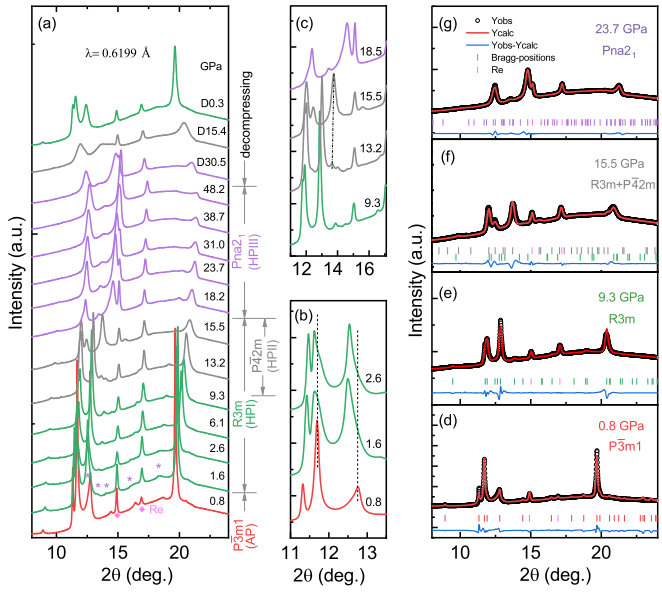

FIG. 3. (a) Synchrotron XRD patterns of $NiGa_2S_4$ powders at selected pressures. The asterisks (∗) denote the new diffraction peaks characteristic for HP I and the diamonds (◊) for the rhenium gasket. (b) and (c) Zoom-in views for the transitions near 1.6 and 15.5 GPa. (d)–(g) Typical refinement results at 0.8, 9.3, 15.5, and 23.7 GPa by using the Le Bail method. The red, green, gray, and purple vertical ticks at the bottom correspond to the calculated Bragg positions of various phases with the $P\bar{3}m1$, $R3m$, $P\bar{4}2m$, and $Pna2_1$ symmetries, respectively.

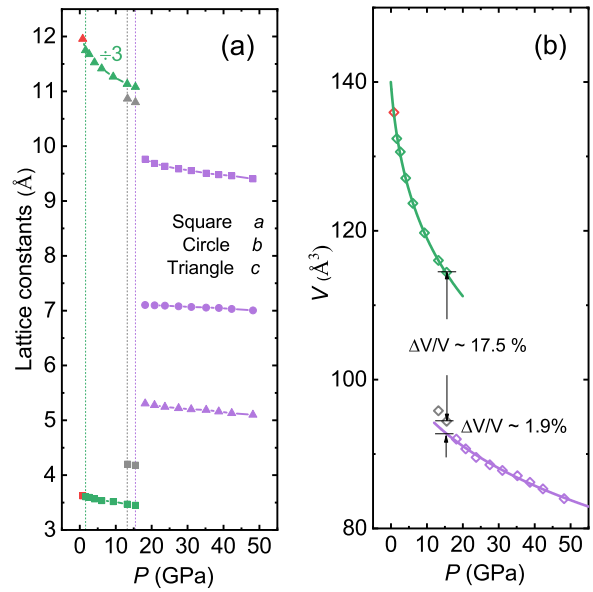

FIG. 4. (a) Lattice constants and (b) unit-cell volume as a function of pressure for $NiGa_2S_4$. The scatters in red, green, gray, and purple present different phases of $P\bar{3}m1$, $R3m$, $P\bar{4}2m$, and $Pna2_1$, respectively. The solid lines are the fitting results by the third-order Birch-Murnaghan formula.

as indicated by the returning insulating behavior at 17 GPa as shown in Fig. 2(a). This rapid, reversible phase transition between insulating and metallic states suggests that $NiGa_2S_4$ system show possibility of applications in Mott memory devices, with the help of the pressure.

B. Synchrotron x-ray diffraction

To better understand the metallization in $NiGa_2S_4$, the *in situ* synchrotron XRD measurements were performed on crushed crystal powders up to 48.2 GPa at room temperature. The representative diffraction patterns are presented in Fig. 3(a). For 0.8 GPa, Le Bail refinements were carried out using the FULLPROF package, $P\bar{3}m1$ symmetry of $NiGa_2S_4$ perfectly indexes all reflections with $a = b = 3.62$, $c = 11.96$ Å, a little smaller than the ambient lattice parameters [19], see Fig. 3(d). At 1.6 GPa, several new peaks emerge as indicated by the asterisk (∗) in Fig. 3(a) and the original strong peaks show distinct downshift as depicted in Fig. 3(b), further, the Le bail fitting failed when using the starting $P\bar{3}m1$ symmetry. These observations indicate that a structural phase transition occurs at this very low pressure (labeled as HP I). The XRD profiles remained up to 13.2 GPa from where a new peak set in at 13.7° and immediately followed by two dramatic changes at 15.5 and 18.2 GPa, respectively, which can be clearly seen in Fig. 3(c). Combing the following Raman data, we, consequently, suppose the system passes through an intermediate phase (labeled as HP II) to enter into one high-pressure phase (labeled as HP III) in the range of 13.2–18.2 GPa, obviously this seems coincident with the IMT results.

Considering the feasible models for the new high-pressure structures in $NiGa_2S_4$, we focus on the discovered structures in AB_2X_4 family, which adopt a plethora of crystal structure types, most of which belong to the cubic spinel or tetragonal structures and rare members with layered structures of rhombohedral (space-group $R3m$, No.160) or trigonal ($P\bar{3}m1$) symmetries, and some high-pressure phases crystallized with orthorhombic symmetry. According to the number of octahedral (Ω) and tetrahedral (τ) cationic sites, it was assumed that the layered structures ($\Omega + 2\tau$) are intermediate between the spinel ($2\Omega + \tau$) and the tetragonal structures (3τ) [30]. We have carried out the Le Bail refinement and found that the Bragg peaks in the XRD patterns can be well indexed by the layered rhombohedral $R3m$ phase ($Z = 3$) for the HP I phase, the tetragonal $P\bar{4}2m$ phase (space-group No.75, $Z = 2$) for the HP II phase, and orthorhombic $Pna2_1$ phase (space-group No. 33, $Z = 4$) for the HP III phase, respectively. Figures 3(d)–3(g) display the Le Bail refinement results for pressure of 9.3, 15.5, and 23.7 GPa, respectively. With decompressing, the sample undergoes a reversible structural change, and recovers to the final HP I phase as shown in Fig. 3(a). The structural phase transitions reported here pave a way to study the pressure-tuned properties of the $NiGa_2S_4$-type compounds.

The lattice parameters and unit-cell volume of $NiGa_2S_4$ were extracted from Le Bail refinements of the XRD data and plotted in Figs. 4(a) and 4(b) as a function of pressure. Above lower pressure of 1.6 GPa, a sliding of unit layers along the [110] axis makes the axis c triple and leads to the transition from $P\bar{3}m1$ to $R3m$, meanwhile, the lattice constants and unit-cell volume shows a continuous decrease. There exists a large volume difference between the $R3m$ and the $P\bar{4}2m$ phases, it shows a collapse of ∼17.5% at 15.5 GPa, and one negligible reduction is also obtained between the $P\bar{4}2m$ and the $Pna2_1$

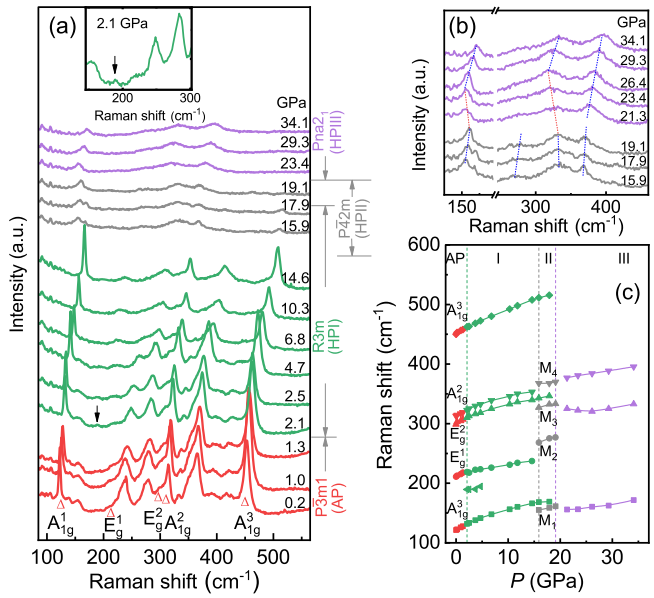

FIG. 5. Pressure evolutions of Raman spectra of $NiGa_2S_4$ at selected pressures. The different colored lines correspond to various phases as marked on the side. (b) Zoom-in view in the vicinity of transitions from $P\bar{4}2m$ to $Pna2_1$ phases. (c) Pressure dependence of Raman frequencies in $NiGa_2S_4$.

phases. The equations of state for high-pressure phases were fitted by using the third-order Birch-Murnaghan formula [31],

$$P = \frac{3}{2}B0[(V0/V)^{7/3} - (V0/V)^{5/3}]\left\{1 + \frac{3}{4}(B1-4)\left[(V0/V)^{2/3}-1\right]\right\},$$

where $V0$, $B0$, and $B1$ are the volume, bulk modulus $-V/(dV/dP)$, and first-order derivative of the bulk modulus at zero pressure, respectively. The fitting yields $V0 = 139.7$ Å^3, $B0 = 22.7$, and $B1 = 11.8$ GPa for the HP I phase, and $V0 = 102.2$ Å^3, $B0 = 95.5$, and $B1 = 11.2$ GPa for the HP III phase. The orthogonal-type phase for $NiGa_2S_4$ exhibits a much larger incompressibility than the trigonal-type phase.

C. Raman scattering

The structural phase transitions in pressurized $NiGa_2S_4$ are also supported by Raman-scattering measurements at room temperature. $NiGa_2S_4$ crystallizes with $P\bar{3}m1$ symmetry, which corresponds to the D_{3d} point group. Group-symmetry analysis predicts the optical phonon modes of $NiGa_2S_4$ as follows:

$$\Gamma = 3A_{1g} + 3E_g + 3A_{2u} + 3E_u,$$

out of which $3A_{2u}$ and $3E_u$ are the infrared active modes while $3A_{1g}$ and $3E_g$ are the Raman active modes, A_{1g} belongs to the interlayer vibrations of two Ga-S1 layers along c axis, and E_g corresponding to the vibrations of S atoms on the $a-b$ plane. Figure 5(a) shows the Raman-scattering spectra evolution of $NiGa_2S_4$ with pressure. For 0.2 GPa, five of the six Raman active modes are observed in our configuration, including the A^1_{1g}, E^1_g, E^2_g, A^2_{1g}, and A^3_{1g} modes at 121, 206, 296, 313, and 450 cm^{-1}, respectively, which are similar to the ambient pressure data [26], whereas one low-wavenumber E_g mode was beyond our equipment limit. There are also some broad low intensity Raman-inactive vibrations modes, which belong to the infrared active modes activated by a local loss of inversion center due to the presence of S vacancies, the whole Raman profile is consist with previous report in Ref. [26]. Among this, the phonons E^1_g and A^3_{1g} provide more information because it involves the movement of S2, which forming the S2-Ni-S2 triangular lattice, they can affect the C_3 symmetry of the S2-Ni-S2 bonds and the nearest-neighbor exchange interactions J_1.

At lower pressure, all Raman modes show coincident blueshifts. Above 2.1 GPa, one additional slender peak emerges at 188.3 cm^{-1}, which can be clearly seen in the inset of Fig. 5(a). This is probably due to the lower symmetry of $R3m$ compared to $P\bar{3}m1$, for example, there are seven or eight Raman modes observed in $R3m$-type $ZnIn_2S_4$ [32]. Figure 5(c) depicts the pressure dependence of Raman frequencies of $NiGa_2S_4$, all Raman modes keep continuous blueshifts in the whole range of AP and HP I phases. Above 15.9 GPa, four new broad peaks (M1–M4) emerge as well as the overall Raman intensity suddenly drop, nevertheless the old weak E^1_g, E^2_g, and A^3_{1g} modes remained until 17.9 GPa. These observations lie in excellent agreement with above XRD results which revealed the $R3m \rightarrow P\bar{4}2m$ transition near 15.5 GPa, whereas the sharp reduction in Raman intensity can be accounted for the insulator-to-metal transition observed in electrical measurements. With further compressing to 21.3 GPa as clearly seen in Fig. 5(b), the M1 and M3 Raman modes show contrary redshifts, which could be due to the structural instability near $P\bar{4}2m \rightarrow Pna2_1$ transition as detected in the XRD data. Above 26.4 GPa, the ordinary blueshifts reemerge. Thus, the Raman-scattering results match well with the former XRD and IMT, despite slight deviation of critical pressure values, which can be influenced by the different PTMs employed in different measurements (see Sec. II).

Therefore, a path route of structural changes of $P\bar{3}m1 \rightarrow R3m \rightarrow P\bar{4}2m \rightarrow Pna2_1$ is proposed in $NiGa_2S_4$ under high pressure. The IMT seems entangled with the structural changes from trigonal to tetragonal phases where a 17.5% collapse in the unit-cell volume is obtained. In real materials, there exist multiple degrees of freedom as the driving force of the IMT, such as the charge degrees of freedom by bandwidth-controlled and filling-controlled mechanism, spin degrees of freedom by collapse of the magnetic moment due to an increase incrystal-field splitting, and orbital degrees of freedom. Pressure-induced first-order IMTs usually lead to a number of changes, including orbital repopulation [33], moment reduction [34] and volume collapse [35], these changes may occur simultaneously, or sequentially over a range of volumes, any of these may be accompanied by a structural or isosymmetric structural phase transition [34]. In this report, $NiGa_2S_4$ shows an inversible IMT entangled with a structural phase transition between the HP I phase and the HP II phase, it is worth it to further study the structural, electronic, or possible magnetic transformations combined with calculations to reveal the underlining real mechanism of Mott transition in $NiGa_2S_4$.

IV. CONCLUSIONS

To summarize, we experimentally studied the high-pressure behavior of $NiGa_2S_4$ using electrical transport, synchrotron XRD, and Raman spectroscopy measurements. Combining XRD patterns and Raman spectra, three structural phase transitions were identified at 1.6, 15.5, and 18.2 GPa, leaving four structural regions of AP, HP I, HP II, and HP III with possible symmetries of $P\bar{3}m1$, $R3m$, $P\bar{4}2m$, and $Pna2_1$, respectively. One reversible IMT was observed accompanied with the second structural change from $R3m$ to $P\bar{4}2m$. The metallic phase shows no superconductivity until 1.8 K. These findings enrich the studies of the Mott insulator $NiGa_2S_4$ within tuning parameters, and prompt further understanding the complex interaction in $NiGa_2S_4$ by means the pressure.

ACKNOWLEDGMENTS

We are grateful for financial support from the National Key R&D Program of China (Grants No. 2022YFA1602603 and No. 2018YFA0305704), the Key Project of Natural Scientific Research of Universities in Anhui Province (Grants No. KJ2021A0064 and No. KJ2021A0068), the National Natural Science Foundation of China (Grants No. 12004004, No. U19A2093, No. 12204004, No. U1932152, and No. 12174395), the Users with Excellence Program of Hefei Center CAS (Grant No. 2021HSC-UE008). Yonghui Zhou was supported by the Youth Innovation Promotion Association CAS (Grant No. 2020443). The high-pressure synchrotron x-ray diffraction experiments were performed at the beamline BL15U1, Shanghai Synchrotron Radiation Facility.

[1] P. A. Lee, N. Nagaosa, and X.-G. Wen, Doping a Mott insulator: Physics of high-temperature superconductivity, Rev. Mod. Phys. **78**, 17 (2006).

[2] C. Broholm, R. J. Cava, S. A. Kivelson, D. G. Nocera, M. R. Norman, and T. Senthil, Quantum spin liquids, Science **367**, 263 (2020).

[3] A. P. Ramirez, Geometric frustration: Magic moments, Nature (London) **421**, 483 (2003).

[4] L. Balents, Spin liquids in frustrated magnets, Nature (London) **464**, 199 (2010).

[5] A. Lauchli, F. Mila, and K. Penc, Quadrupolar Phases of the $S = 1$ Bilinear-Biquadratic Heisenberg Model on the Triangular Lattice, Phys. Rev. Lett. **97**, 087205 (2006).

[6] Y. Kamiya and C. D. Batista, Magnetic Vortex Crystals in Frustrated Mott Insulator, Phy. Rev. X **4**, 011023 (2014).

[7] W. M. Natori, E. C. Andrade, E. Miranda, and R. G. Pereira, Chiral Spin-Orbital Liquids with Nodal Lines, Phys. Rev. Lett. **117**, 017204 (2016).

[8] P. W. Anderson, The resonating valence bond state in La_2CuO_4 and superconductivity, Science **235**, 1196 (1987).

[9] Y. Shimizu, K. Miyagawa, K. Kanoda, M. Maesato, and G. Saito, Spin Liquid State in an Organic Mott Insulator with a Triangular Lattice, Phys. Rev. Lett. **91**, 107001 (2003).

[10] Y. Xu, Y. Sheng, and Y.-f. Yang, Mechanism of the insulator-to-metal transition and superconductivity in the spin liquid candidate $NaYbSe_2$ under pressure, npj Quantum Mater. **7**, 1 (2022).

[11] Y.-T. Jia, C.-S. Gong, Y.-X. Liu, J.-F. Zhao, C. Dong, G.-Y. Dai, X.-D. Li, H.-C. Lei, R.-Z. Yu, G.-M. Zhang, and C.-Q. Jin, Mott transition and superconductivity in quantum spin liquid candidate $NaYbSe_2$, Chin. Phys. Lett. **37**, 097404 (2020).

[12] D. P. Kozlenko, A. F. Kusmartseva, E. V. Lukin, D. A. Keen, W. G. Marshall, M. A. de Vries, and K. V. Kamenev, From Quantum Disorder to Magnetic Order in an $S = 1/2$ Kagome Lattice: A Structural and Magnetic Study of Herbertsmithite at High Pressure, Phys. Rev. Lett. **108**, 187207 (2012).

[13] P. Malavi, S. Pal, D. V. S. Muthu, S. Sahoo, S. Karmakar, and A. K. Sood, Pressure-induced tuning of quantum spin liquid state in $ZnCu_3(OH)_6Cl_2$, Phys. Rev. B **101**, 214402 (2020).

[14] I. Mirebeau, I. N. Goncharenko, P. Cadavez-Peres, S. T. Bramwell, M. J. Gingras, and J. S. Gardner, Pressure-induced crystallization of a spin liquid, Nature (London) **420**, 54 (2002).

[15] L. Forró, R. Gaál, H. Berger, P. Fazekas, K. Penc, I. Kézsmárki, and G. Mihály, Pressure Induced Quantum Critical Point and Non-Fermi-Liquid Behavior in BaVS3, Phys. Rev. Lett. **85**, 1938 (2000).

[16] J. S. Zhou, J. B. Goodenough, and B. Dabrowski, Pressure-induced Non-Fermi-Liquid Behavior of $PrNiO_3$, Phys. Rev. Lett. **94**, 226602 (2005).

[17] D. Durkee, N. Dasenbrock-Gammon, G. A. Smith, E. Snider, D. Smith, C. Childs, S. A. J. Kimber, K. V. Lawler, R. P. Dias, and A. Salamat, Colossal Density-Driven Resistance Response in the Negative Charge Transfer Insulator MnS_2, Phys. Rev. Lett. **127**, 016401 (2021).

[18] D. Bhoi, J. Gouchi, N. Hiraoka, Y. Zhang, N. Ogita, T. Hasegawa, K. Kitagawa, H. Takagi, K. H. Kim, and Y. Uwatoko, Nearly Room-Temperature Ferromagnetism in a Pressure-Induced Correlated Metallic State of the Van Der Waals Insulator $CrGeTe_3$, Phys. Rev. Lett. **127**, 217203 (2021).

[19] S. Nakatsuji, Y. Nambu, H. Tonomura, O. Sakai, S. Jonas, C. Broholm, H. Tsunetsugu, Y. Qiu, and Y. Maeno, Spin disorder on a triangular lattice, Science **309**, 1697 (2005).

[20] S. Nakatsuji, Y. Nambu, K. Onuma, S. Jonas, C. Broholm, and Y. Maeno, Coherent behaviour without magnetic order of the triangular lattice antiferromagnet $NiGa_2S_4$, J. Phys.: Condens. Matter **19**, 145232 (2007).

[21] H. Takeya, K. Ishida, K. Kitagawa, Y. Ihara, K. Onuma, Y. Maeno, Y. Nambu, S. Nakatsuji, D. E. MacLaughlin, A. Koda, and R. Kadono, Spin dynamics and spin freezing behavior in the two-dimensional antiferromagnet $NiGa_2S_4$ revealed by Ga-NMR, NQR and μSR measurements, Phys. Rev. B **77**, 054429 (2008).

[22] C. Stock, S. Jonas, C. Broholm, S. Nakatsuji, Y. Nambu, K. Onuma, Y. Maeno, and J. H. Chung, Neutron-scattering Measurement of Incommensurate Short-Range Order in Single Crystals of the $S = 1$ Triangular Antiferromagnet $NiGa_2S_4$, Phys. Rev. Lett. **105**, 037402 (2010).

[23] E. M. Stoudenmire, S. Trebst, and L. Balents, Quadrupolar correlations and spin freezing in $S = 1$ triangular lattice antiferromagnets, Phys. Rev. B **79**, 214436 (2009).

[24] H. Tsunetsugu and M. Arikawa, Spin Nematic Phase in $S = 1$ Triangular Antiferromagnets, J. Phys. Soc. Jpn. **75**, 083701 (2006).

[25] S. Bhattacharjee, V. B. Shenoy, and T. Senthil, Possible ferro-spin nematic order in $NiGa_2S_4$, Phys. Rev. B **74**, 092406 (2006).

[26] M. E. Valentine, T. Higo, Y. Nambu, D. Chaudhuri, J. Wen, C. Broholm, S. Nakatsuji, and N. Drichko, Impact of the Lattice on Magnetic Properties and Possible Spin Nematicity in the $S = 1$ Triangular Antiferromagnet $NiGa_2S_4$, Phys. Rev. Lett. **125**, 197201 (2020).

[27] J. M. Honig and J. Spałek, Electronic properties of $NiS_{2-x}Se_x$ single crystals: From magnetic Mott-Hubbard insulators to normal metals, Chem. Mater. **10**, 2910 (1998).

[28] S. Friedemann, H. Chang, M. B. Gamża, P. Reiss, X. Chen, P. Alireza, W. A. Coniglio, D. Graf, S. Tozer, and F. M. Grosche, Large fermi surface of heavy electrons at the border of mott insulating state in NiS_2, Sci. Rep. **6**, 25335 (2016).

[29] Y. Nambu, M. Ichihara, Y. Kiuchi, S. Nakatsuji, and Y. Maeno, Synthesis and characterization of the quasi-two-dimensional triangular antiferromagnets $Ni_{1-x}MxGa_2S_4$ (M = Mn, Fe, Co, Zn), J. Cryst. Growth **310**, 1881 (2008).

[30] F. J. Manjon, I. Tiginyanu, and V. Ursaki, *Pressure-Induced Phase Transitions in AB2 × 4 Chalcogenide compounds* (Springer, Berlin, 2014).

[31] F. Birch, Finite strain isotherm and velocities for single-crystal and polycrystalline NaCl at high pressures and 300° K, J. Geophys. Res. Solid Earth **83**, 1257 (1978).

[32] S. A. Lopez-Rivera, L. Martinez, B. Fontal, W. Giriat, and F. Medina, Raman study of a $ZnIn_2S_4$ layered compound, Semicond. Sci. Technol. **10**, 645 (1995).

[33] Y. Z. Zhang, H. O. Jeschke, and R. Valenti, Two Pressure-Induced Transitions in TiOCl: Mott Insulator to Anisotropic Metal, Phys. Rev. Lett. **101**, 136406 (2008).

[34] J. Kunes, A. V. Lukoyanov, V. I. Anisimov, R. T. Scalettar, and W. E. Pickett, Collapse of magnetic moment drives the Mott transition in MnO, Nature Mater. **7**, 198 (2008).

[35] S. Wang, J. Chen, L. Wu, and Y. Zhao, Giant Viscoelasticity Near Mott Criticality in $PbCrO_3$ with Large Lattice Anomalies, Phys. Rev. Lett. **128**, 095702 (2022).